Biosensors and Bioelectronics 92 (2017) 186–191

Contents lists available at ScienceDirect

Biosensors and Bioelectronics

journal homepage: www.elsevier.com/locate/bios

Rapid detection and quantification of Enterovirus 71 by a portable surface plasmon resonance biosensor

Briliant Adhi Prabowo[a,f,1], Robert Y.L. Wang[b,d,1], Muhammad Khari Secario[a], Po-Ting Ou[b], Azharul Alom[a], Jia-Jung Liu[a], Kou-Chen Liu[a,c,d,e,*]

[a] Department of Electronic Engineering, Chang Gung University, Taoyuan 33002, Taiwan
[b] Department of Biomedical Sciences, College of Medicine, Chang Gung University, Taoyuan 33302, Taiwan
[c] Center for Biomedical Engineering, Chang Gung University, Taoyuan 33302, Taiwan
[d] Division of Pediatric Infectious Disease, Department of Pediatrics, Chang Gung Memorial Hospital, Linkou 33305, Taiwan
[e] Department of Materials Engineering, Ming Chi University of Technology, New Taipei City 24301, Taiwan
[f] Research Center for Informatics, Indonesian Institute of Sciences, Bandung 40135, Indonesia

ARTICLE INFO

Keywords:
EV71
SPR
Sensor
VP1
Virus
Quantification method

ABSTRACT

This study presents the first report on a label-free detection and rapid quantification method for human enterovirus 71 (EV71) using a portable surface plasmon resonance (SPR) system. The SPR sensor instrument was configured to run on low power in a miniaturized platform to improve the device portability for a wider application both in laboratories and in the field. A color tunable organic light emitting diode in red spectrum was attached on a trapezoidal prism for the disposable light source module. The SPR signal processing using integration area under the reflectivity curve is applied for optimum signal to noise ratio (SNR) enhancement. The major capsid protein VP1 of EV71 was selected as the biomarker target in the detection study. The experimental time required for the EV71 quantification was reduced from 6 days using the conventional viral plaque assay to several minutes using the proposed method. The study results establish a detection limit of approximately 67 virus particles per milliliter (vp/ml) of EV71 in a Dulbecco's modified Eagle's medium. The VP1 detection in the portable SPR biosensor had a detection limit of approximately 4.8 pg/ml in the PBS buffer. Therefore, the proposed direct EV71 viral particle quantification method can be rapidly performed in real time, with high sensitivity and less labor and without assays or fluorescence.

1. Introduction

The most notable cases of hand-foot-and-mouth diseases, in which the virus leads to morbidity and/or mortality, are those of the Enterovirus 71 (EV71). EV71 has spread in the East and Southeast Asian regions (Shahmahmoodi et al., 2008; Wong et al., 2012), including in Taiwan (Chang, 2008; Liu et al., 2014a). Nevertheless, some cases occurred as low-level outbreaks in Africa, Europe, and the United States (Yip et al., 2013). The common transmission routes are fecal–oral and respiratory. Primary infection with EV71 leads to a viral replication in the mucosa tissue around the respiratory or gastro-intestinal tract (Wong et al., 2012). Subsequently, the infection moves from the periphery to the central nervous system (Lin et al., 2008). Moreover, the infection may be difficult to diagnose because its symptoms are similar to those of other neuro-invasive diseases, such as aseptic meningitis and acute flaccid paralysis (Wong et al., 2012). Therefore, a further study on EV71 viral detection is essential to advance progress on this disease.

In clinical diagnosis, the EV71 virus can be detected by examining the viral genomic RNA through enzyme-linked immunosorbent assay (ELISA) to detect specific antiviral antibodies in the patient's specimen (Liu et al., 2014a; Lin et al., 2014). The isolation of EV71 from the patient's specimen is the first process required for a definitive diagnosis of the enterovirus. However, this technique is time-consuming. Moreover, the necessary growth period lasts for at least six days, which hinders crucial diagnoses during outbreaks. Therefore, developing a method of serologically testing paired mild- and severe-phase serum samples is the foundation of effective EV71 diagnosis. In a laboratory, EV71 viral particles are detected using a plaque-forming assay, in which the virus titer is calculated as the number of plaques (Tsou et al., 2013; Wang et al., 2013b). This plaque-forming quantification method requires another five days. Therefore, this conventional method is also

* Corresponding author at: Department of Electronic Engineering, Chang Gung University, 259 Wenhua 1st Road, Guishan, Taoyuan 33002, Taiwan.
E-mail address: jacobliu@mail.cgu.edu.tw (K.-C. Liu).
[1] These authors contributed equally to this work.

http://dx.doi.org/10.1016/j.bios.2017.01.043
Received 28 October 2016; Received in revised form 11 January 2017; Accepted 20 January 2017
Available online 21 January 2017
0956-5663/

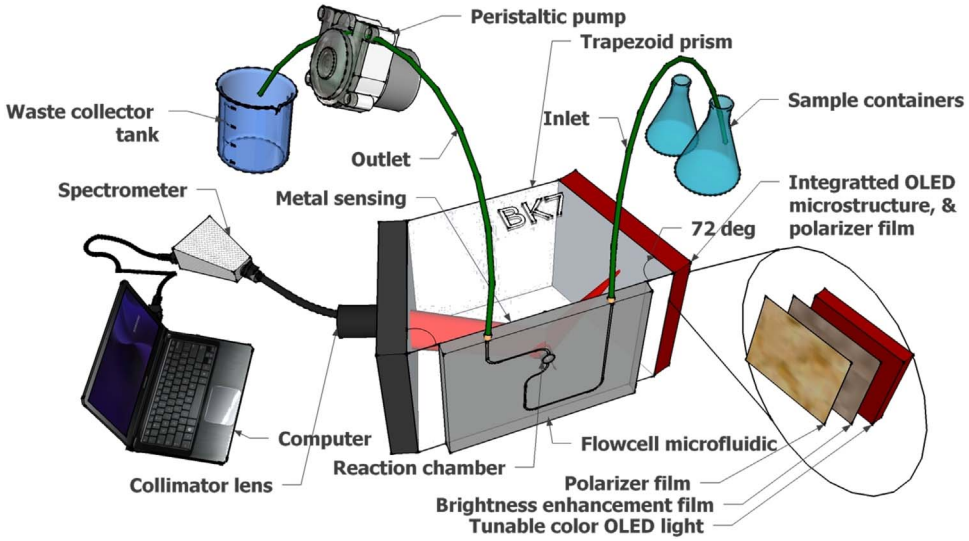

Fig. 1. Configuration of the portable SPR sensor instrument using a color tunable OLED integrated with brightness enhancement and a polarizer microstructure (Prabowo et al., 2014, 2016). (For interpretation of the references to color in this figure, the reader is referred to the web version of this article.)

an impractical diagnostic approach to outbreaks. Several reports demonstrated other EV71 viral quantification methods. For example, the detection of the EV71 viral proteins using a specific antibody (i.e., ELISA) significantly reduces the analysis time by several hours based on the antibody incubation time (Lin et al., 2014; Liu et al., 2011). This method is more easily implemented and also more reproducible compared to the plaque-forming assay. However, the time required to detect ELISA is still several hours. Several groups also reported other indirect viral quantification methods based on the reverse transcription-polymerase chain reaction (RT-PCR) (Chen et al., 2014a; Hayden et al., 2013; Lui and Tan, 2014; Tan et al., 2008). This approach offers excellent viral detection reproducibility. However, some of the following issues in this process need to be considered: it is dependent on reverse transcription; it is imprecise and inefficient; and the material and assay performance characteristics tend to vary during and after the calibration (Hayden et al., 2013; Sanders et al., 2013). Accordingly, simpler methods of directly detecting viral particles to accurately detect EV71, such as by using transmission electron microscopy (TEM), were reported. Nevertheless, these methods have several drawbacks, such as their high cost, time-consuming procedure, and instrument immobility. Flow cytometry is also another method of directly detecting a viral particle (Y. Liu et al., 2014b). This method can reduce the analysis time down to 10 min. However, the flow cytometry quantification method can only detect viral particles in the range of approximately 10^5 to 10^9 viral particles/ml, which is still quite high as a detection limit for accurate measurements. Another approach uses surface-enhanced Raman scattering (SERS) for direct viral particle detection. This method was reported to be able to detect extremely low concentrations of viral particles because of its high sensitivity to localized surface plasmon resonance phenomena on the metal nanoparticle. However, this technology still lacks reproducibility, portability, and real-time detection capability (Chang et al., 2011; Sivashanmugan et al., 2013; Tripp et al., 2008; Yao et al., 2012).

The biomarker detection of EV71 using a SPR biosensor is required for rapid identification during an outbreak. In addition, the Capsid protein VP1 occupies the predominant protein proportion on the EV71 surface. The protein also plays a particular role in conjunction with the etiological agents that cause hand and mouth diseases. Furthermore, VP1 proteins contain the important epitopes recognized by neutralizing antibodies (Gao et al., 2016; Hendry et al., 1999; Miao et al., 2009). The VP1 of EV71 is preferred as the biomarker target in this SPR sensor detection study because of this specific profile.

There are limited reports related to the VP1 detection using a biomarker method, particularly involving a biosensor. Studies on the VP1 detection were reported by several groups using well-known methodologies, such as ELISA (Gao et al., 2016; Zhang et al., 2016), reverse transcription–loop-mediated isothermal amplification (Ding et al., 2014), and RT-PCR (Fan et al., 2013). Nevertheless, the detection methods reported in these studies still require assays or labeling. The present study proposes a rapid, real-time, and label-free detection of the VP1 biomarker from the EV71 virus using an SPR biosensor.

The SPR phenomena on the interface between gold and the measured medium establish an evanescent wave that penetrates up to 200 nm inside the measured medium (Homola, 2008) and is sensitive to the refractive indices shifting on the gold surface. In contrast, the small particle of the EV71 structure has a physical diameter of approximately 30–32 nm (Liu et al., 2011; Plevka et al., 2012). Consequently, the evanescent wave penetration depth can cover all the particles of the EV71 virus on the gold sensing layer. The number of EV71 particles is represented by the refractive indices of the medium on the gold surface. The portable SPR instrument has several advantages presented as follows: it is low-voltage, lightweight, and palm-sized. Therefore, the EV71 quantification can be performed at low-cost clinics or point-of-care facilities in isolated areas, in the field, or in an emergency vehicle. The significant contribution offered by this proposed method is the direct, rapid, and non-labor intensive viral detection of EV71. In addition, the modular and disposable component of the SPR sensor can be used for other purposes, such as for an organic light source (Prabowo et al., 2014). The SPR sensor protocols offer high sensitivity, real-time detection, and free assays and fluorescence (Su et al., 2012). The SPR signal processing using integration area under the reflectivity curve is applied for optimum SNR enhancement. Therefore, the SPR sensor method offers a very practical approach for use during outbreak periods. Based on our knowledge to date, this study presents the first report on the EV71 quantification and detection using a portable SPR biosensor.

2. Materials and method

The portable SPR instrument system and its measurement methodology were designed and constructed by our group (Prabowo et al., 2014, 2016). Tunable color organic light emitting diodes (OLEDs) (Ultimate Image Corp., Taiwan) were used to apply polychromatic light. Figs. 1 and S1 show the configuration of the portable SPR sensor instrument.

2.1. Direct viral quantification

This study proposes a direct viral quantification of EV71 purified from the culture medium. The crystal structure of EV71 was coated by VP1, VP2, VP3, and VP4 (Plevka et al., 2012), which contained amino acid chains (Spain-Santana et al., 2001). The previous study reported that the amino acid can be attached to the gold particle because of the relative binding strengths of the amine group and gold (Hoefling et al., 2010; Links, 2011; Pakiari and Jamshidi, 2007). In the case of a sulfide containing the amino acid, such as cysteine (Wang et al., 2011), the binding force can even be stronger because of covalent interactions (Sperling and Parak, 2010). Our direct detection method utilized a rich variety of amino acid structures in EV71 to directly immobilize the viral particle to the gold metal sensing component. We eliminate the surface chemistry of the gold layer for the purpose of quantification. The whole experimental process can be up to 24 h shorter because of the eliminated procedures.

2.2. Viral plaque assay

The conventional viral plaque assay (VPA) method of the EV71 quantification was compared to the SPR methods for experimental confirmation. The rhabdomyosarcoma (RD) cells were seeded in six-well plates at 4×10^5 cells per well, followed by an overnight incubation in a DMEM solution containing 10% FBS to form a monolayer. The supernatants of the culture medium samples from the EV71-infected cells and the 10-fold serial dilutions of the sucrose gradient fractions were prepared in a serum-free DMEM medium before infection. Monolayered RD cells were incubated in serum-free DMEM medium for 1 h before adding 0.5 ml of the 10-fold dilutions and 0.5 ml of the serum-free DMEM medium. The RD cells were incubated for an additional hour to stimulate the infection. The cells were then washed with the serum-free medium, and 2 ml of 0.3% agarose (Invitrogen, Thermo Fisher Scientific, MA, USA) in the serum-free medium was added to each well. The seeded plates were incubated at room temperature for 30 min to solidify the agarose. The cells were then cultured at 37 °C for four days. Subsequently, the cells were mixed with 2 ml of 10% formaldehyde and incubated at room temperature for 30 min before the overlaid agarose was removed. The cells were stained with a solution of 0.5% crystal violet, 1.85% formalin, 50% ethanol, and 0.85% NaCl (Sigma Aldrich, MO, USA) for 2 min, then washed with deionized water. The viral particles were calculated as the number of plaques (1 ml/0.5 ml) times the serial dilution factor and were expressed in plaque-forming units per milliliter (PFU/ml).

2.3. Gold sensing fabrication and functionalization

Different metal sensors were used for the experiments in this study (i.e., a gold monolayer sensor and a bimetallic Ag/Au sensor) following our established method (Prabowo et al., 2016, 2014). For the VP1 target detection, the metal sensing was functionalized at room temperature for 20 h using 1 mM of thiol-terminated polyethylene glycol (PEG) (Nanocs, NY, USA) and 9 mM of thiol-free PEG to configure the spacing of the antibody immobilization. The amine coupling reagent kit of 1-ethyl-3-(3-dimethylaminopropyl)-carbodiimide hydrochloride (EDC), N-hydroxysuccinimide (NHS), and 1.0 M ethanolamine-HCl (pH 8.5) (ETH) was purchased from Biacore (GE Life Sciences, USA).

2.4. Cell line, virus strain, and viral infection

RD cells were cultured in a DMEM medium (Gibco-BRL, Carlsbad, CA, USA), then supplemented with 10% FBS (Gibco-BRL, Carlsbad, CA, USA), 100 units of penicillin, 24 mM of sodium bicarbonate (Sigma-Aldrich, St. Louis, MO, USA), and 50 μg/ml of streptomycin (Gibco-BRL, Carlsbad, CA, USA). The cultured cells were maintained at 37 °C in a 5% CO_2 atmosphere. EV71 (Enterovirus 71 strain TW/2272/98 polyprotein gene, GenBank: AF119795.2) were amplified in the RD cells, and a plaque assay was used to measure the titers. For virus infection, the RD cells were washed with PBS and incubated in a serum-free medium for 1 h before the viral infection. The cells infected with EV71 were then stirred every 15 min for 1 h at 37 °C. The infected cells were finally washed with PBS, cultured in the complete medium as described earlier, and stored at −80 °C.

2.5. Antibody, plasmid, and protein expression and purification

The antibody targeted in this experiment was the anti-Enterovirus 71 MAB979 (Merck, Darmstadt, Germany). The MBP-VP1 protein was conducted using the following method: 1) the VP1 DNA fragment was amplified by the PCR primers 5′-ATGCGGATCCATGGGAGATAGGGTGGCAGATG-3′ (forward, *Bam*HI) and 5′-GATCAAGCTTTCAGAGAGTGGTAATTGCTGTG-3′ (reverse, *Hin*dIII), then cloning into pMAL-p5X vectors digested with *Bam*HI and *Hin*dIII; 2) the pMAL-p5X-VP1 was transformed into *Escherichia coli*; the MBP-VP1 protein expression was achieved by the induction of isopropyl-D-thiogalactopyranoside (IPTG); and 3) the recombinant protein was purified by amylose affinity resin in vitro. The non-specific protein target was extracted from a non-structural protein of the Zika virus (NS1).

2.6. Methodology

The signal processing method applied in this research integrated the signal under the reflectance intensity curve in the wavelength range from approximately 20 nm before to approximately 20 nm after the reflectivity dip. The area was calculated using the Riemann sums approach (Taylor, 2006). The SPR signal integration of the 20 nm wavelength range under the reflectivity curve before the minimum dip was referred to as S_A, while the corresponding integration area after the reflectivity dip was referred to as S_B. The reflectivity profile shifted to the upper wavelength position when a higher refractive index value of the medium flowed into the chamber. Therefore, the S_A value increased, whereas the S_B value decreased. The total SPR signal was calculated from S_A-S_B. Fig. 2 illustrates the signal processing methodology applied in this study. This method improves noise reduction to accommodate the photon fluctuation from the incident light. The additional calculation significantly enhanced the total signal. Consequently, the signal to the noise ratio (SNR) of the instrument was enhanced.

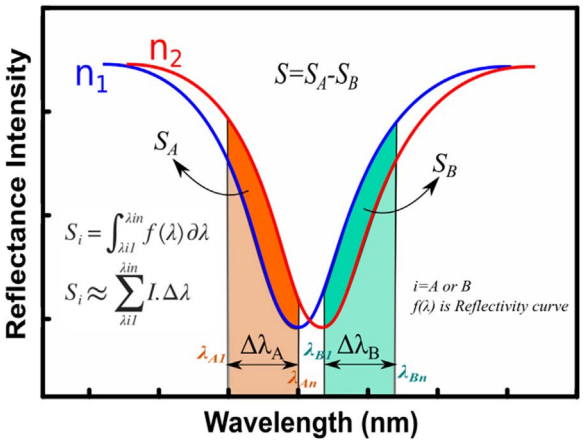

Fig. 2. SPR signals (S) are processed from the intensity integrated in the desired wavelength region of the SPR reflectivity profile. S_A and S_B represent the SPR signals in the wavelength ranges before and after the reflectivity dip, respectively. S is calculated from S_A-S_B, where S_A is positive because the signal slope is positive, and S_B is negative because the signal slope is negative as the refractive indices shift.

3. Results and discussion

The advantage of using an OLED is the stability it offers for an extended performance operation. The OLED has a large substrate over which to integrate the heat dissipation. Therefore, self-heating is not a critical circumstance in OLED technology (Chung et al., 2009). Fig. S1 shows the wavelength spectrum of the organic light source used in this study. The wavelength of the light source's red spectra peaked at 615 nm. The stability performance was measured for up to 2 h (inset of Fig. S1) along the full-width half maximum wavelength range (FWHM=590–630 nm). The coefficient of variation (CV) of the stability test was calculated from the standard deviation (σ) divided by the average (ā) of the signal (i.e., approximately 1.2%). The CV is an essential parameter for selecting the preferred light source representing the uniformity of all points across the test's entire real-time lighting operation performance. A lower CV value indicates a uniform and a stable light source performance.

3.1. Viral quantification

Fig. S2(a) depicts the direct visual detection of the purified EV71 immobilized to the gold surface. The purified EV71 particles in the DMEM medium were dropped on the gold surface and allowed to adhere for 5 min before washing with pure DMEM solution. This gold substrate was then observed using a field emission scanning electron microscope (FESEM) to obtain a visual proof of the EV71 affinity for the gold surface. The viral particles and the structure of EV71 were observed through transmission electron microscopy (TEM) to obtain a visual illustration of the viral particle size and the capsid protein responsible for the direct binding to the gold monolayer in the SPR sensor (Fig. S2(b)). We observed the EV71 viral particle using a gold mesh substrate for the TEM. The first figure shows the EV71 viral particle with a medium magnification of the microscope. The second one presents the details of a single EV71 particle with high magnification. Fig. S2(a) and (b) provide a visual proof of the direct immobilization of the EV71 to the gold layer for the quantification procedures.

The initial measurement of the SPR sensor performance was the reflectivity test shown in Fig. S3(a). The test indicates the strength of the light absorption at the sensing interface caused by the SPR phenomena. The shifts in the reflectivity profile caused by the differences in the refractive indices in the medium can be conceptually recognized based on the reflectivity curve generated by the SPR sensor performance test.

The negative control sample was the DMEM medium with zero concentration of the EV71 viral particle, which flowed for 5 min. This sample exhibited the minimum reflectivity dip at approximately 618 nm. The DMEM medium with the lowest concentration, in which the cultured virus was diluted for 16 times, was later flowed for 5 min. The SPR reflectivity was significantly shifted to a higher wavelength. Subsequently, different samples with increased concentrations, in which the cultured virus was diluted for 8, 4, 2, and 1 times, were flowed for 5 min each. From the reflectivity curves in Fig. S3(a), it is difficult to recognize the minimum reflectivity dip in terms of wavelength, particularly as the signals gradually shift as the sample concentrations increase, with small variations in the minimizing wavelength from 624 to 628 nm. This drawback can be overcome by utilizing a high-resolution spectrometer, which requires a costly investment. The proposed methodology described in Section 2.4 was applied to eliminate this issue. We can easily recognize the signal shift in the wavelength ranges of $\Delta\lambda_A$=598–618 nm and $\Delta\lambda_B$=628–648 nm in terms of both wavelength and intensity magnitude. The high-resolution spectrometer was not necessary to investigate the signal's intensity magnitude. Hence, the sensor's resolution was considered to be entirely dependent on the light source stability shown in Fig. S1 inset.

The diluted samples were examined for the EV71 viral particle quantification using the SPR sensor. The numbers of the EV71 viral particle concentrations were obtained by VPA, which was described in Section 3.4. The number of EV71 viral particles were 8.125×10^5, 1.625×10^6, 3.25×10^6, 6.5×10^6, and 1.3×10^7 vp/ml, for 16, 8, 4, 2, and 1 dilutions, respectively. The real-time SPR signals were monitored in the wavelength ranges $\Delta\lambda_A$ and $\Delta\lambda_B$, which corresponded to S_A and S_B, respectively. The S_A signal increased as the reflectivity dip shifted to the higher wavelength because $\Delta\lambda_A$ was located within the wavelength range before the reference reflectivity dip. In contrast, S_B incrementally decreased with respect to the samples' refractive indices because the $\Delta\lambda_B$ wavelength range was located in the range after the reference reflectivity dip. The real-time SPR signals S_A and S_B were plotted in Fig. S3(b). The figure shows the signal differences between each of the different EV71 viral particle concentrations. S_{A-B} was calculated from S_A-S_B, resulting in the normalized S_{A-B} (Fig. S3(c)). S_{A-B} more clearly displayed the signal enhancement compared to the single real-time signals represented by S_A and S_B. Moreover, the noise value will be reduced because $\sigma_{A-B}=\sqrt{=}\sigma_A^2+\sigma_B^2$). Consequently, the SPR signal S_{A-B} resulted in a higher SNR compared to the single $\Delta\lambda$ monitoring method.

The SPR signal responses S_{A-B} of each solution containing different concentrations of the EV71 viral particles were normalized and plotted in Fig. 3. The curve was then fitted using a dose–response model variable, as described in the figure notes.

We utilized different types of metal sensing layers for the optimum estimation of the detection limit for the viral quantification at even very low viral particle concentrations: a Au monolayer and a Ag/Au bimetallic layer. Fig. 3 shows the results for which. The resonance wavelength occurred at 639 nm and 614 nm with the Au monolayer and the Ag/Au bimetallic layer, respectively, because of the high refractive index of the DMEM used as the solution medium. Therefore, the quality factor of the reflectivity profile (Prabowo et al., 2014) in the bimetallic structure showed a more favorable value because the resonance wavelength position matched the peak of the OLED spectrum, as shown in Fig. 3 inset. Consequently, and as shown in Fig. 3, the bimetallic sensing structure illustrated a significantly higher SPR signal compared to the Au monolayer.

The fitting formula is $Y=N/(1+10^{S(L-X)})$, where N is the maximum signal level; S is the slope of the fitting curve; and L is the logarithmic value of x when Y=N/2. The detection limit was the concentration value, at which the signal was estimated at 3σ in relation to the reference signal positioned on the fitting curve. In other words, the 3σ

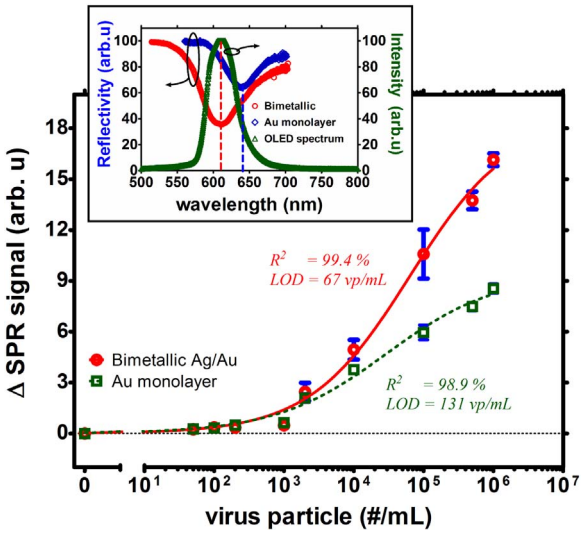

Fig. 3. Curve fitting of the measured series concentrations of the EV71 virus particle samples following the variable slope dose–response model. The inset shows a comparison of the resonance dip positions of the different sensing structures: the Au monolayer and the Au/Ag bimetallic layer (the relative standard deviation is listed in Table S1).

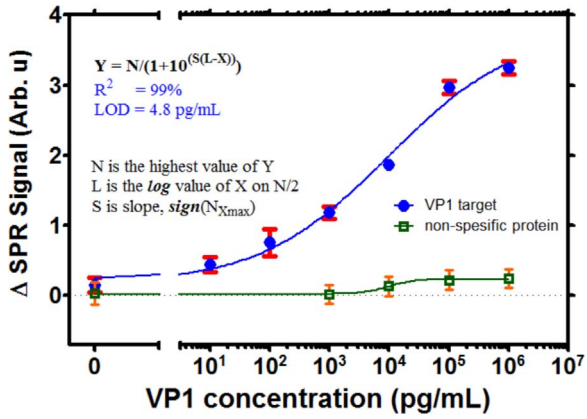

Fig. 4. Calculated VP1 detection limit. The green square curve shows the signal level of the non-specific protein target (the relative standard deviation is listed in Table S2). (For interpretation of the references to color in this figure legend, the reader is referred to the web version of this article.)

value was tracked at the fitted curve to determine the concentration of the detection limit. Fig. 3 also presents the statistical information represented by the fitted curve. The σ was approximately 0.27 and 0.09 for the Au and Au/Ag sensing layers, respectively. These values established the detection limits at 131 and 67 vp/ml for the Au and Ag/Au sensing layers, respectively. The limit of the detection performance was almost four order smaller compared to the previous SERS viral detection method (Sivashanmugan et al., 2013).

3.2. VP1 biomarker detection

The VP1 detection in EV71 with the SPR platform was divided into four main steps as follows: surface activation, antibody immobilization, blocking, and biomarker target detection. Fig. S4(a) shows the real-time SPR measurements of surface activation, antibody immobilization, and blocking. First, the acetate buffer (pH 5.0) was flowed to the reaction chamber. The thiol-PEG brush was then activated by a mixture of the NHS/EDC reagent for 15–20 min. The NHS/EDC mixture reagent has a higher refractive index value compared to the acetate buffer. Thus, the measurements indicated rapid incremental changes in the SPR signal. The chemical modification reached a steady state after several minutes, as indicated by the saturated signal level. Subsequently, the mixture was washed with acetate for 5 min. The antibody solution in the acetate was then injected into the chamber to perform the immobilization step over a period of 30 min. The SPR signal gradually increased, thereby indicating the binding of the antibodies in the functionalized thiol-PEG layer. After which, the acetate wash was performed to remove unbound antibodies from the solution, followed by a PBS buffer injection. Subsequently, the blocking protocol was implemented using an ETH reagent to cover the activated PEG brush; several parts of which did not occupy the antibody. Finally, a PBS buffer wash determined the reference signal level of the detection target.

Fig. S4(b) illustrates the detection of the VP1 series concentration targeted with the SPR platform. The sequential concentrations in the PBS solution were 10 pg/ml, 100 pg/ml, 1 ng/ml, 10 ng/ml, 100 ng/ml, and 1 μg/ml. The PBS wash was performed after 20 min for every concentration measurement. The system was also tested with a non-specific protein target for the specificity comparison. The signal level showed a slight increase compared to the reference signal. Fig. 4 plots the specific signal levels after the wash following the dose–response stimulation model. The calculated detection limit was 4.8 pg/ml considering that the noise of the reference signal was 0.1.

Table 1 summarizes the studies related to the viral quantification and EV71 detection methods. This comparison showed that the novel and alternative method for the direct EV71 viral particle quantification proposed in this paper provides comparable quantification results. Moreover, the study demonstrated the proof of concept of this novel VP1 biomarker detection method.

4. Conclusions

This study presented rapid, simple, real-time, sensitive, and less labor-intensive EV71 viral particle quantification and VP1 biomarker detection methods using a portable SPR sensor-based organic light source. The SPR signal processing using integration area under the reflectivity curve is applied for optimum signal to noise ratio (SNR) enhancement. This proposed viral quantification is essential to the ongoing study of EV71, particularly in Taiwan, where this virus

Table 1
Summary of the acknowledged methods of viral quantification and EV71 detection.

Techniques	Principle	Time	Reproducibility	Real-time	Labor work	Quantified marker	Ref.
VPA	Infection unit	Several days	Poor	No	High	5×10^{-6} $TICD_{50}$ 10^6 PFU $>10^4$ PFU	Liu et al. (2011) Lee et al. (2015) Chen et al. (2014b), Lin et al. (2008)
ELISA	Antigen detection	Several hours	Good	No	Moderate	15 μg/ml 0.650 OD_{450}	Lin et al. (2014) Wang et al. (2004)
HPLC	Antigen detection	Days	Excellent	No	High, high experienced	0.2 mg/ml 0.32–3.1 μg/mg	Huang et al. (2013) C.-Y. Wang et al. (2013a)
PCR	Gene expression	Several hours	Excellent	Yes (for RT-PCR)	High, high experienced	160 μg/ml 5 viral copies 25 viral copies 0.4 PFU	Liu et al. (2011) Tan et al. (2008) Lui and Tan (2014) Spain-Santana et al. (2001)
TEM	Viral particles	Several days	Good	No	High, high experienced	~10^6/ml 12.5 mg/ml ~50 mg/l	Liu et al. (2011) Lin et al. (2014) Chung et al. (2010)
Flow cytometry	Antigen, particles of infected cells	Minutes	Good	Yes	High	6–243 infected cell $>5\times10^4$ infected cell >122 cell/mm^3	Nishimura et al. (2009) Du et al. (2015) Wang et al. (2003)
SERS	Particles of infected cells, antigen	Minutes	Poor	No	Moderate, high experienced	10^6 PFU/ml $>10^{-10}$ M	Chang et al. (2011), Sivashanmugan et al. (2013) Yao et al. (2012)
SPR sensor	Viral particles, antigen	Minutes	Good	Yes	Moderate	67 vp/ml 4.8 pg/ml	This work

remains a serious threat. Compared to conventional EV71 quantification methods, such as ELISA and VPA, the SPR sensor-based quantification method demonstrates a significantly lower detection limit (i.e., as low as 67 vp/ml and 4.8 pg/ml) for the VP1 detection in the PBS solution. This quantification and detection method also offers high reproducibility and a less labor-intensive measurement alternative. The future work on this method will investigate its potential in measuring EV71 infection in clinical samples to evaluate the method's specificity and feasibility.

Acknowledgments

This research was supported and funded by the Chang Gung Memorial Hospital Research Project (CMRPD3E0231-2), the Taiwan National Science Council (NSC 10-0232-5B18-2006), and the Taiwan National Research Program for Biopharmaceuticals (NRPB 10-0IDP-1008-2) to K.-C. Liu and in part by the Chang Gung Memorial Hospital Research Fund (CMRPD1E0411-2 and CMRPD1F0281-2) to Robert Y.L. Wang.

Appendix A. Supporting material

Supplementary data associated with this article can be found in the online version at http://dx.doi.org/10.1016/j.bios.2017.01.043.

References

Chang, C.W., Liao, J.D., Shiau, A.L., Yao, C.K., 2011. Sens. Actuators B Chem. 156, 471–478.
Chang, L.-Y.Y., 2008. Pediatr. Neonatol. 49, 103–112.
Chen, Q., Hu, Z., Zhang, Q., Yu, M., 2014a. J. Virol. Methods 196, 139–144. http://dx.doi.org/10.1016/j.jviromet.2013.11.003.
Chen, Q., Hu, Z., Zhang, Q., Yu, M., Deng, C.-L., Yeo, H., Ye, H.-Q., Liu, S.-Q., Shang, B.-D., Gong, P., Alonso, S., Shi, P.-Y., Zhang, B., 2014b. J. Virol. Methods 88, 11915–11923.
Chung, C.Y., Chen, C.Y., Lin, S.Y., Chung, Y.C., Chiu, H.Y., Chi, W.K., Lin, Y.L., Chiang, B.L., Chen, W.J., Hu, Y.C., 2010. Vaccine 28, 6951–6957.
Chung, S., Lee, J.-H., Jeong, J., Kim, J.-J., Hong, Y., 2009. Appl. Phys. Lett. 94, 253302.
Ding, X., Nie, K., Shi, L., Zhang, Y., Guan, L., Zhang, D., Qi, S., Ma, X., 2014. J. Clin. Microbiol. 52, 1862–1870.
Du, X., Wang, H., Xu, F., Huang, Y., Liu, Z., Liu, T., 2015. Mol. Med. Rep. 12, 953–959.
Fan, X., Jiang, J., Liu, Y., Huang, X., Wang, P., Liu, L., Wang, J., Chen, W., Wu, W., Xu, B., 2013. Virus Genes 46, 1–9.
Gao, C., Ding, Y., Zhou, P., Feng, J., Qian, B., Lin, Z., Wang, L., Wang, J., Zhao, C., Li, X., Cao, M., Peng, H., Rui, B., Pan, W., 2016. Sci. Rep. 6, 21979.
Hayden, R.T., Gu, Z., Ingersoll, J., Abdul-Ali, D., Shi, L., Pounds, S., Caliendo, A.M., 2013. J. Clin. Microbiol. 51, 540–546.
Hendry, E., Hatanaka, H., Fry, E., Smyth, M., Tate, J., Stanway, G., Santti, J., Maaronen, M., Hyypiä, T., Stuart, D., 1999. Structure 7, 1527–1538.
Hoefling, M., Iori, F., Corni, S., Gottschalk, K.-E., 2010. Langmuir 26, 8347–8351.
Homola, J., 2008. Chem. Rev. 108, 462–493.
Huang, S., Lyu, Y., Qing, X., Wang, W., Tang, L., Cheng, K., Wang, W., 2013. Biotechnol. Lett. 35, 1845–1852.
Lee, P.-H., Liu, C.-M., Ho, T.-S., Tsai, Y.-C., Lin, C.-C., Wang, Y.-F., Chen, Y.-L., Yu, C.-K., Wang, S.-M., Liu, C.-C., Shiau, A.-L., Lei, H.-Y., Chang, C.-P., 2015. PLoS One 10, e0116278.
Lin, C.-W., Wu, C.-F., Hsiao, N.-W., Chang, C.-Y., Li, S.-W., Wan, L., Lin, Y.-J., Lin, W.-Y., 2008. Int. J. Antimicrob. Agents 32, 355–359.
Lin, S.-Y., Chung, Y.-C., Chiu, H.-Y., Chi, W.-K., Chiang, B.-L., Hu, Y.-C., 2014. J. Biosci. Bioeng. 117, 366–371.
Links, D.A., 2011. Soft Matter 7, 2113–2120.
Liu, C.C., Guo, M.S., Lin, F.H.Y., Hsiao, K.N., Chang, K.H.W., Chou, A.H., Wang, Y.C., Chen, Y.C., Yang, C.S., Chong, P.C.S., 2011. PLoS One 6.
Liu, C.-C., Chow, Y.-H., Chong, P., Klein, M., 2014a. Vaccine 32, 6177–6182.
Liu, Y., Zhang, Z., Zhao, X., Yu, R., Zhang, X., Wu, S., Liu, J., Chi, X., Song, X., Fu, L., Yu, Y., Hou, L., Chen, W., 2014b. Viral Immunol. 27, 267–276.
Lui, Y.L.E., Tan, E.L., 2014. J. Virol. Methods 207, 200–203.
Miao, L.Y., Pierce, C., Gray-Johnson, J., DeLotell, J., Shaw, C., Chapman, N., Yeh, E., Schnurr, D., Huang, Y.T., 2009. J. Clin. Microbiol. 47, 3108–3113.
Nishimura, Y., Wakita, T., Shimizu, H., Shimojima, M., Tano, Y., Miyamura, T., 2009. Nat. Med. 15, 794–797.
Pakiari, A.H., Jamshidi, Z., 2007. J. Phys. Chem. A 111, 4391–4396. http://dx.doi.org/10.1021/jp070306t.
Plevka, P., Perera, R., Cardosa, J., Kuhn, R.J., Rossmann, M.G., 2012. Science 336, 1274.
Prabowo, B.A., Chang, Y.-F., Lee, Y.-Y., Su, L.-C., Yu, C.-J., Lin, Y.-H., Chou, C., Chiu, N.-F., Lai, H.-C., Liu, K.-C., 2014. Sens. Actuators B Chem. 198, 424–430.
Prabowo, B.A., Su, L., Chang, Y., Lai, H., Chiu, N.-F., Liu, K.-C., 2016. Sens. Actuators B 222, 1058–1065.
Sanders, R., Mason, D.J., Foy, C.A., Huggett, J.F., 2013. PLoS One 8.
Shahmahmoodi, S., Mehrabi, Z., Eshraghian, M.R., Azad, T.M., Tabatabaie, H., Yousefi, M., Farrokhi, K., Gouya, M.M., Esteghamati, A., Moosavi, T., Zahraie, M., Rad, K.S., Shokati, Z., Nategh, R., 2008. J. Clin. Virol. 42, 409–411.
Sivashanmugan, K., Liao, J. Der, You, J.W., Wu, C.L., 2013. Sens. Actuators, B Chem. 181, 361–367.
Spain-Santana, T.A., Marglin, S., Ennis, F.A., Rothman, A.L., 2001. J. Med. Virol. 65, 331–339.
Sperling, R.A., Parak, W.J., 2010. Philos. Trans. A. Math. Phys. Eng. Sci. 368, 1333–1383.
Su, L.-C., Chang, C.-M., Tseng, Y.-L., Chang, Y.-F.Y.-S., Li, Y.-C., Chou, C., 2012. Anal. Chem. 84, 3914–3920.
Tan, E.L., Yong, L.L.G., Quak, S.H., Yeo, W.C.A., Chow, V.T.K., Poh, C.L., 2008. J. Clin. Virol. 42, 203–206.
Taylor, M.E., 2006. American Mathematical Society, Rhode Island, USA.
Tripp, R.A., Dluhy, R.A., Zhao, Y., 2008. Nano Today 3, 31–37.
Tsou, Y.-L., Lin, Y.-W., Chang, H.-W., Lin, H.-Y., Shao, H.-Y., Yu, S.-L., Liu, C.-C., Chitra, E., Sia, C., Chow, Y.-H., 2013. PLoS One 8, e77133.
Wang, C.-Y., Huang, S.-C., Lai, Z.-R., Ho, Y.-L., Jou, Y.-J., Kung, S.-H., Zhang, Y., Chang, Y.-S., Lin, C.-W., 2013a. Evid. Based Complement. Altern. Med. 2013, 591354. http://dx.doi.org/10.1155/2013/591354.
Wang, J., Fan, T., Yao, X., Wu, Z., Guo, L., Lei, X., Wang, J., Wang, M., Jin, Q., Cui, S., 2011. J. Virol. 85, 10021–10030. http://dx.doi.org/10.1128/JVI.05107-11.
Wang, R.Y.L., Kuo, R.-L., Ma, W.-C., Huang, H.-I., Yu, J.-S., Yen, S.-M., Huang, C.-R., Shih, S.-R., 2013b. Virology 443, 236–247.
Wang, S.-M., Lei, H.-Y., Huang, K.-J., Wu, J.-M., Wang, J.-R., Yu, C.-K., Su, I.-J., Liu, C.-C., 2003. J. Infect. Dis. 188, 564–570.
Wang, S.Y., Lin, T.L., Chen, H.Y., Lin, T.S., 2004. J. Virol. Methods 119, 37–43.
Wong, K.T., Ng, K.Y., Ong, K.C., Ng, W.F., Shankar, S.K., Mahadevan, A., Radotra, B., Su, I.J., Lau, G., Ling, A.E., Chan, K.P., Macorelles, P., Vallet, S., Cardosa, M.J., Desai, A., Ravi, V., Nagata, N., Shimizu, H., Takasaki, T., 2012. Neuropathol. Appl. Neurobiol. 38, 443–453.
Yao, C.K., Liao, J. Der, Chang, C.W., Lin, J.R., 2012. Sens. Actuators, B Chem. 174, 478–484.
Yip, C.C.Y., Lau, S.K.P., Woo, P.C.Y., Yuen, K.Y., 2013. Emerg. Health Threats J. 6, 19780.
Zhang, A., Xiu, B., Zhang, H., Li, N., 2016. J. Int. Med. Res. 44, 287–296.